

Research article

Enhancing interfacial interactions of cocontinuous poly(lactic acid)/polyethylene blends using vinylsilane grafted carbon nanotubes as generic reactive compatibilizers

Bin Wang¹, Qiaolie Zheng¹, Mengjia Li¹, Sisi Wang¹, Shanglin Xiao¹, Xiping Li¹, Hesheng Liu^{2*}

¹Key Laboratory of Urban Rail Transit Intelligent Operation and Maintenance Technology & Equipment of Zhejiang Province, College of Engineering, Zhejiang Normal University, 321004 Jinhua, People's Republic of China

²School of Mechatronics and Vehicle Engineering, East China Jiaotong University, 330013 Nanchang, People's Republic of China

Received 26 November 2021; accepted in revised form 25 January 2022

Abstract. Vinylsilane grafted carbon nanotubes (VCNTs) can act as reactive compatibilizers for cocontinuous poly(lactic acid)/high-density polyethylene (PLA/HDPE) blends, with the aid of organic peroxides initiated radical reactions. The reactively compatibilized PLA/HDPE/VCNTs blend nanocomposites exhibit strong interfacial interactions, as can be reflected by the remarkably increased storage modulus at low frequencies. Due to strong interfacial interactions, the VCNTs act as highly efficient nucleating agents for the PLA component. With 2.0 wt% of VCNTs, the crystallinity of PLA component reaches a value of 33.8% after melt cooling, and thus cold crystallization can no longer be observed upon heating. Thanks to the high crystallinity of the PLA component, the reactively compatibilized blend nanocomposite with 2.0 wt% of VCNTs shows a much higher elastic modulus than those of pristine PLA/HDPE blends and uncompatibilized blend nanocomposites in the temperature range of 60 to 80 °C. Moreover, the reactively compatibilized blend nanocomposites exhibit an obvious increase trend in tensile strength with increasing the content of VCNTs, due to stronger interfacial interactions. This work provides a generic strategy for compatibilizing and reinforcing immiscible polymer blend nanocomposites using reactive carbon nanotubes.

Keywords: polymer composites, rheology, interfacial interactions, thermal properties

1. Introduction

Polymer blending is an evergreen technique for exploring new materials. To endow polymer blends with superior and multifunctional properties, it is essential to control their morphology and interfacial interactions [1, 2]. Many of the polymers are thermodynamically immiscible with each other. Thus, compatibilizers are usually needed for manipulating the morphology and interfacial interactions of polymer blends [3–6]. Highly efficient and universally applicable compatibilizers are consistent pursuing in both academics and industry.

Recently, the bio-based polymer blends and blend nanocomposites have attracted extensive attention [7, 8]. Poly(lactic acid) (PLA) is one of the most important bio-based and biodegradable polyesters, which possesses high mechanical strength but inherent brittleness [9]. Thus, the PLA is usually toughened by means of blending with a second polymer, such as polyethylene (PE) [10–12]. The PE is one of the commonly used polymers, which can also be produced from renewable resources except for producing from oil [13, 14]. This naturally leads to the expectations that much promising high performance

*Corresponding author, e-mail: hsliu@ecjtu.edu.cn
© BME-PT

and multifunctional materials would be exploited via blending PLA and PE.

Various compatibilizing strategies were developed for the PLA/PE blends since the two were thermodynamically immiscible. PLA–PE block copolymers were synthesized to improve the miscibility between PLA and PE components [15, 16]. The PLA–PE block copolymers were expected to decrease the interfacial tension and enhance the interfacial interactions via each block entangling with the molecular chains of the corresponding component. Besides the PLA–PE block copolymers, copolymers of ethylene–glycidyl methacrylate (E-GMA) and ethylene–methyl acrylate–glycidyl methacrylate (EMA-GMA) were employed as reactive compatibilizers for the PLA/PE blends [17, 18]. It was revealed that end groups of PLA chains reacted with epoxide groups of the compatibilizers to form graft copolymers, which obviously enhanced the interfacial interactions.

Apart from the copolymers, Janus particles can also act as highly efficient compatibilizers for polymer blends [19–21]. Typically, for a given polymer blend, the corresponding Janus particles can be obtained by grafting the molecular chains of each component to the surface of certain nanoparticles. That is, for PLA/PE blends, specific Janus particles grafted with both PLA and PE chains should be designed and synthesized. Differently, a recently reported vinylsilane grafted graphene arouses the anticipation that vinylsilane grafted nanoparticles may act as more universal ‘Janus particles’ to compatibilize polymer blends [22]. By simply initiating the radical reactions via organic peroxides, vinylsilane grafted nanoparticles are expected to bond the chains of both components to *in-situ* compatibilize the blends. Thus, the authors are inspired to compatibilize the PLA/PE blends using vinylsilane grafted nanoparticles, especially for the PLA/PE blends with cocontinuous morphology. Cocontinuous PLA/PE blends are usually prepared on purpose to realize electric or thermal functions [23], while their miscibility and mechanical properties are marginalized.

In this work, vinylsilane grafted carbon nanotubes (VCNTs) were synthesized and were employed to compatibilize the cocontinuous PLA/high-density PE (HDPE) (50/50, w/w) blends with the aid of dicumyl peroxide (DCP). The morphology and microstructures of PLA/HDPE/VCNTs blend nanocomposites were analyzed, and their compatibilizing

mechanism was revealed. The enhanced interfacial interactions in the blend nanocomposites were evidenced by linear rheological and thermal dynamic analysis results.

2. Experimental

2.1. Materials

Carbon nanotubes (CNTs, XFM07) were purchased from Xianfeng Nano Technology Co., Ltd, Nanjing, China. Both PLA and HDPE granules used in this study were commercially available. The PLA (grade 4032D) with a melt flow index (*MFI*) of $7 \text{ g} \cdot 10 \text{ min}^{-1}$ (2.16 kg, 210 °C) was produced by NatureWorks Co., Ltd, Blair, USA; while the HDPE (grade 5218EA) with an *MFI* of $16 \text{ g} \cdot 10 \text{ min}^{-1}$ (2.16 kg, 190 °C) was produced by Dushanzi Petrochemical Co., Ltd, Karamay, China. Trichlorovinylsilane was purchased from Aladdin Chemistry Co., Ltd, Shanghai, China. The DCP was purchased from Titan Scientific Co., Ltd, Shanghai, China. Sodium hydroxide (NaOH), ethanol, and 30% hydrogen peroxide (H_2O_2) were all produced by Xilong Chemical Co., Ltd, Shantou, China. Potassium bromide (KBr) was produced by Macklin biochemical Co., Ltd, Shanghai, China. Chloroform was produced by Jincheng reagent Co., Ltd, Kunshan, China. All the chemical reagents were analytically pure grade and were used as received.

2.2. Preparation of VCNTs

The pristine CNTs (1 g) were dispersed into 400 ml of NaOH solution with a concentration of $10 \text{ mol} \cdot \text{l}^{-1}$, by means of an ultrasonic bath. Then, 4 ml of H_2O_2 was dropped into the CNTs/NaOH solution under magnetic stirring, followed by a reaction at room temperature for 48 h [24]. After the reaction, the solution was centrifuged using distilled water several times till neutral. The hydroxylated CNTs suspension was thus obtained.

The obtained hydroxylated CNTs suspension was stirred in an ice bath for 0.5 h, followed by adding 8 ml of trichlorovinylsilane drop-by-drop using an injection syringe. After that, the suspension was transferred into an oil bath for a reaction at 80 °C for 3 h under magnetic stirring. The reacted suspension was centrifuged several times till neutral, and the VCNTs were thus obtained. After freeze-drying, the VCNTs powders were collected for the following melt compounding process.

2.3. Melt compounding and sample preparation

The PLA granules were dried in a vacuum oven for 24 h at 80 °C, and then were dry mixed with HDPE granules at a weight ratio of 50/50. Further dry mixing was performed via adding VCNTs and DCP (dissolved in 2 ml ethanol) to PLA/HDPE mixtures. The contents of VCNTs were set as 0, 0.5, 1.0, and 2.0 wt% to that of PLA/HDPE mixtures, respectively. The weight fraction of DCP was fixed at 0.2% to that of PLA/HDPE mixtures. PLA/HDPE/VCNTs/DCP mixtures were melt compounded using an internal mixer (HAAKE PolyLab) for 10 min. The melt temperature was set as 200 °C, and the speed of the rotors was set as 120 rpm. During melt compounding, the DCP was pyrolyzed into free radicals, which would attack both PLA and HDPE molecular chains to form macromolecular radicals. The vinyl groups on the surfaces of VCNTs were expected to react with both PLA and HDPE radicals, resulting in the reactively compatibilized PLA/HDPE/VCNTs blend nanocomposites.

For comparison, PLA/HDPE/VCNTs blend nanocomposites were prepared with the same processing parameters but without the DCP. Furthermore, PLA/HDPE/pristine CNTs blend nanocomposites were prepared with the aid of DCP using the same processing parameters to validate the importance of vinylsilane modification. The as-prepared PLA/HDPE/VCNTs and PLA/HDPE/CNTs blend nanocomposites were denoted as PxVCNTs, PxVCNTs-DCP, and PxCNTs-DCP, respectively; where x indicates the weight fractions of VCNTs or pristine CNTs. The blend nanocomposites were vacuum-dried at 80 °C for 24 h, and then were compression molded into square samples at 200 °C and 10 MPa. Both length and width of the samples are 80 mm, while the thickness is 0.8 mm.

2.4. Characterization

The CNTs and VCNTs were each ground with potassium bromide (KBr) powders and were compression molded into thin sheets. Then, they were each scanned in transmission mode using a Fourier transform infrared spectroscopy (FTIR) instrument (Thermo Nicolet iS5, ThermoFisher, USA). 32 scans were collected at a resolution of 4 cm⁻¹. Raman spectra of both CNTs and VCNTs were collected by a Raman spectrometer (inVia Reflex, Renishaw, UK) at room temperature.

Transmission electron microscopy (TEM) observations of both CNTs and VCNTs were conducted on a TEM instrument (JEM-2100F, JEOL, Japan). The accelerating voltage was set as 200 kV. Ultrathin sections (200 nm) of the blend nanocomposites for TEM observations were cut using a Leica EM UC7 ultramicrotome and were supported by carbon grids.

Thermogravimetry analysis (TGA) was conducted using a synchronous thermal analyzer (STA 8000, PerkinElmer, USA) at a heating rate of 20 °C/min under a nitrogen atmosphere. The testing temperature range was from 30 to 800 °C.

The morphology of the prepared blends and blend nanocomposites were examined using a scanning electron microscopy (SEM) instrument (EM-30PLUS, COXEM, South Korea). The specimens for SEM observations were cryo-fractured in liquid nitrogen. Then, they were immersed in chloroform at 40 °C for 12 h to etch the PLA phase. After being washed by ethanol, the etched specimens were then gold-sputtered for SEM observations.

A rotational rheometer (MCR302, Anton Paar Instrument, Austria) was used to measure the linear rheological behavior of the prepared blends and blend nanocomposites. The dynamic oscillatory shear measurements were carried out using parallel-plate geometry (diameter: 25 mm, gap: 1 mm) at 200 °C under nitrogen flow. The frequency range was set between 0.01 and 100 rad/s. The strain of 0.6% was confirmed to be well in the linear viscoelastic regime via strain sweep prior to each measurement.

The crystallizing and melting behaviors of the prepared blends and blend nanocomposites were examined using a differential scanning calorimetry (DSC, DSC214, Netzsch, Germany). Specimens of about 8 mg were cut from the prepared blend and blend nanocomposite samples and were heated from 40 to 220 °C at a rate of 30 °C/min. After being held for 5 min to eliminate thermal history, they were cooled down to 40 °C at a rate of 10 °C/min, followed by being heated to 220 °C again at a rate of 10 °C/min. The crystallinity of PLA component in the samples was calculated by $(\Delta H_m - \Delta H_{c,c})/(\Delta H_f \cdot C)$, where ΔH_m and ΔH_f are the endothermic enthalpies of PLA component and 100% crystalline PLA, respectively. A value of 93 J·g⁻¹ was taken as the theoretical endothermic enthalpy of PLA [25]. $\Delta H_{c,c}$ is the exothermic enthalpy of PLA during cold crystallization. C is the weight percentage of PLA.

Dynamic mechanical analysis (DMA) was carried out using a DMA instrument (DMA-1, Mettler Toledo, Switzerland). The specimens were 25.0 mm in length, 6.0 mm in width, and 0.8 mm in thickness. They were scanned from 25 to 120 °C by adopting tension mode. The heating rate was 2 °C/min, and the amplitude was 5 μ m. The frequency was fixed at 1 Hz.

Tensile tests were carried out using a universal testing machine (UTM 4024, Shenzhen SUNS, China) at a strain rate of 1 mm/min, at room temperature. Each experiment was repeated five times.

3. Results and discussion

3.1. Synthesis and characterization of VCNTs

Figure 1a schematically shows the synthesis process of VCNTs. Firstly, pristine CNTs were dispersed into

the solutions of NaOH by means of ultrasonication, and then were transformed into hydroxylated CNTs under the catalysis of H_2O_2 [24]. Secondly, the trichlorovinylsilane was instilled into the neutral hydroxylated CNTs suspension and was hydrolyzed into vinyl silanol. Hydroxyl groups on the surface of CNTs react with the vinyl silanol at elevated temperatures [26, 27]. Lastly, the reaction products were centrifuged several times to obtain the VCNTs. Figures 1b and 1c show the TEM micrographs of both pristine CNTs and VCNTs, respectively. It is observed that the surfaces of VCNTs are not so clear as those of pristine CNTs, due to the decoration of vinyl silane. However, the size of CNTs exhibits little change after grafting of vinyl silane. The diameters of both CNTs and VCNTs are approximately in the range of 8–20 nm.

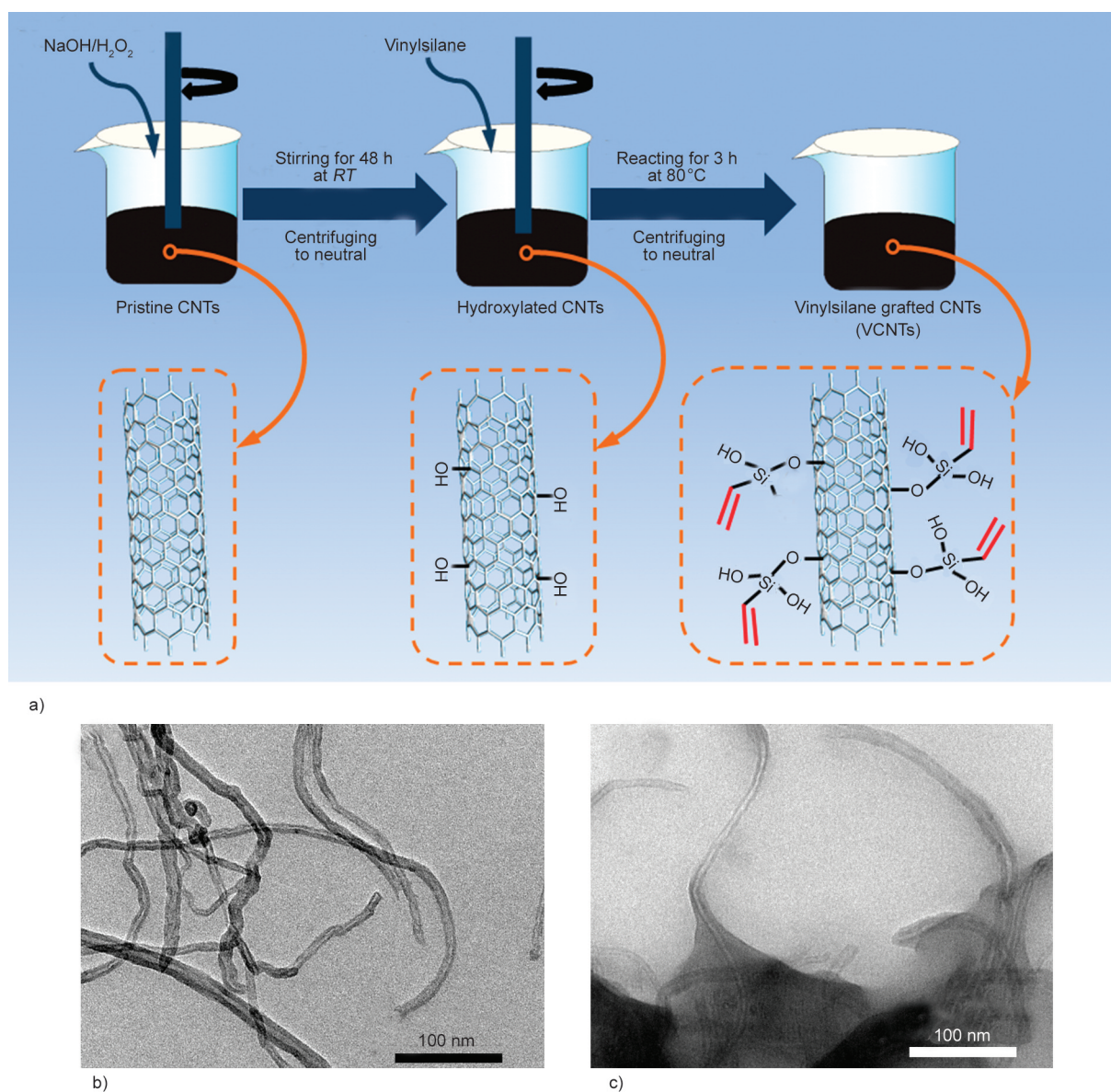


Figure 1. (a) Schematics of synthesizing process of VCNTs; TEM micrographs of (b) CNTs and (c) VCNTs.

Figure 2a shows the FTIR spectra of both pristine CNTs and VCNTs. One observes that new absorbance peaks appear on the spectrum of VCNTs in comparison with that of pristine CNTs. Specifically, the newly emerging absorbance peaks at 1601 and 1126 cm^{-1} correspond to C=C stretching of Si-CH=CH₂ and Si-O-C stretching [28], respectively. This indicates that the vinylsilane is successfully grafted onto the surface of CNTs. The successful grafting of vinylsilane can further be confirmed by the Raman spectra of both pristine CNTs and VCNTs. As can be seen in Figure 2b, the D band and G band of CNTs are located at 1343 and 1596 cm^{-1} , respectively, whereas the D band and G band of VCNTs shift to 1345 and 1588 cm^{-1} , respectively. Moreover, the intensity ratios of G band and D band (I_G/I_D , ratio of peak area) of CNTs and VCNTs are 0.53 and 0.41, respectively. The decreased I_G/I_D of VCNTs is a reflection of defects brought by vinylsilane grafting [29].

Figure 2c exhibits the TGA curves of both CNTs and VCNTs. For the CNTs, obvious weight loss is

observed to begin from 600 °C. However, for the VCNTs, obvious weight loss is observed since 200 °C. The weight loss in the temperature range of 200 to 400 °C can be ascribed to the thermal degradation of both oxygen-containing groups and grafted vinylsilane on the surfaces of VCNTs. According to this, the quantity of oxygen-containing groups and grafted vinylsilane on the surfaces of VCNTs can be estimated as 7.3 wt%.

3.2. Distribution of CNTs and VCNTs in PLA/HDPE blends

Figure 3 selectively exhibits the TEM micrographs of P2.0VCNTs, P2.0VCNTs-DCP, and P2.0CNTs-DCP. The light and dark gray areas correspond to PLA and HDPE phases [30], respectively. It can be clearly seen that, for the P2.0VCNTs, VCNTs dominantly distribute in the HDPE phase (Figure 3a); while for the P2.0VCNTs-DCP, VCNTs are observed to distribute in both PLA and HDPE phases as well as at the interface (Figure 3b). For the P2.0CNTs-DCP, the CNTs mainly distribute in the HDPE phase but

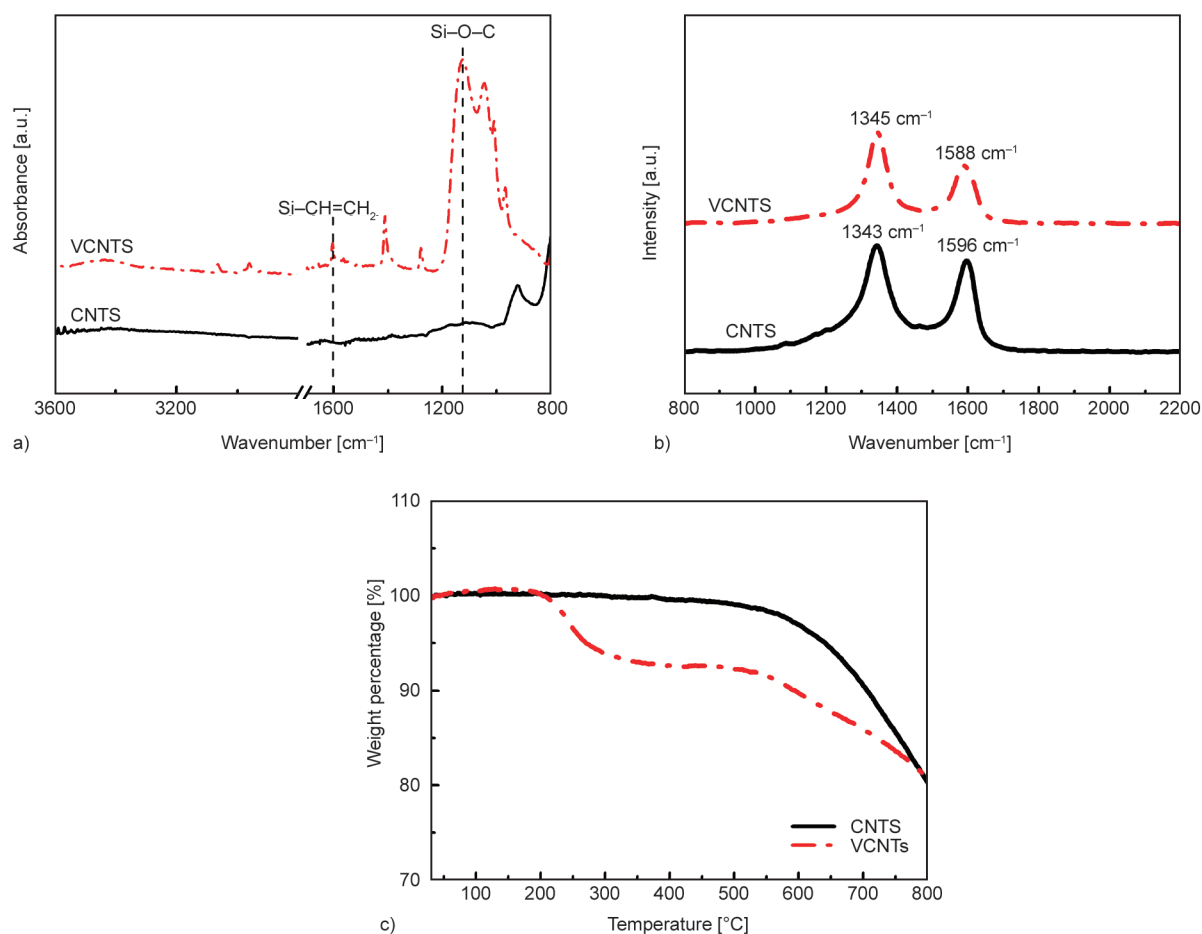


Figure 2. (a) FTIR spectra, (b) Raman spectra, and (c) TGA curves of both CNTs and VCNTs.

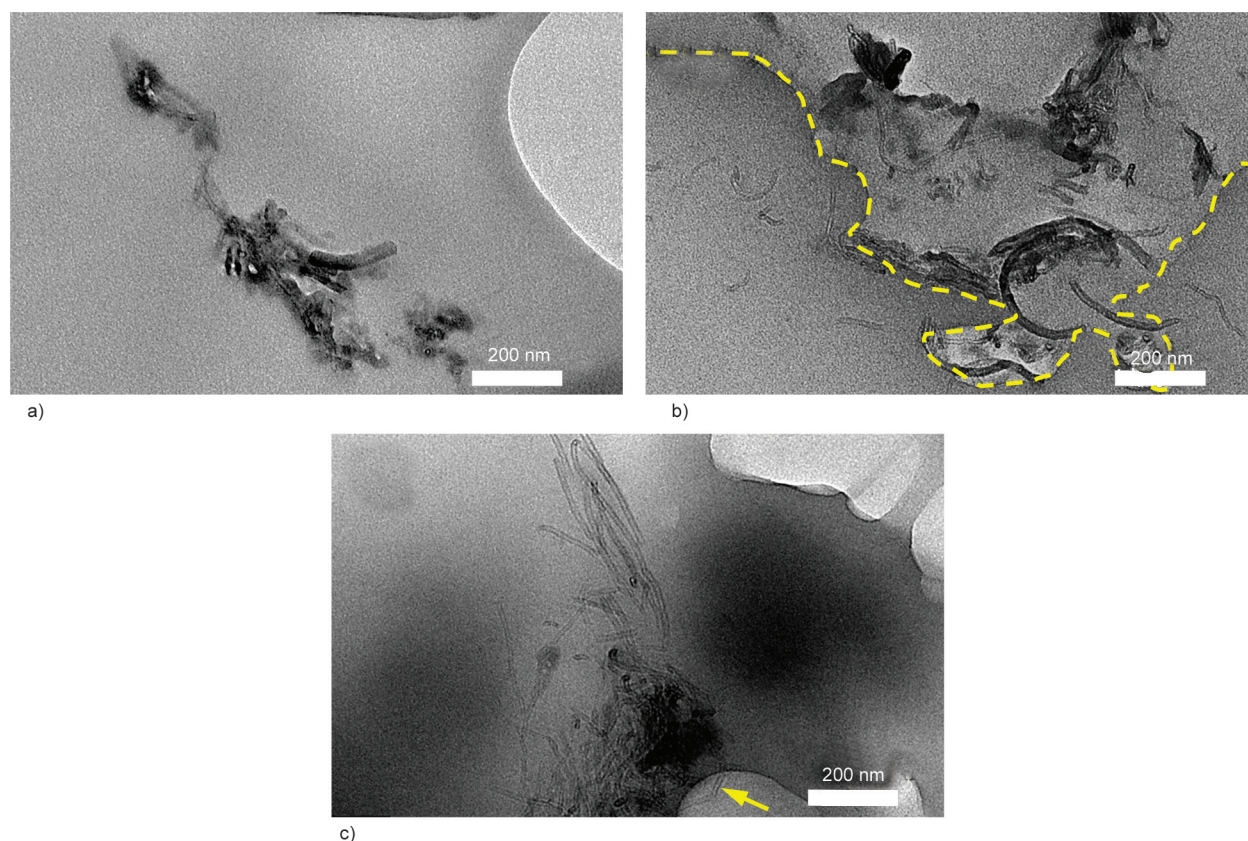


Figure 3. TEM micrographs of (a) PLA/HDPE/VCNTs, (b) PLA/HDPE/VCNTs-DCP, and (c) PLA/HDPE/CNTs-DCP blend nanocomposites with 2 wt% of VCNTs or CNTs.

also in the PLA phase (as illustrated by the arrow in Figure 3c). Moreover, the clusters of CNTs in HDPE phase are observed to be distributed very close to the PLA phase.

During melt compounding, the HDPE component melt first. Thus, the HDPE chains can diffuse around and into the clusters of VCNTs or CNTs earlier than the PLA chains. This leads to the VCNTs or CNTs preferentially distributed in the HDPE phase at the early stage of melt compounding. As the mixing goes, the CNTs tend to migrate toward the PLA phase due to its higher polarity. Thus, clusters of CNTs are observed to distribute in the HDPE phase but located very close to the PLA phase. Furthermore, some CNTs are observed to already migrate into the PLA phase. The VCNTs are prone to stay in the HDPE phase due to their hydrophobic interactions. When VCNTs and DCP are added simultaneously, however, both PLA and HDPE macromolecular radicals are initiated. The affinity of both PLA and HDPE to VCNTs can be improved thanks to the radical reaction. Thus, the VCNTs are observed to distribute in both PLA and HDPE phases as well as at the interface for P2.0VCNTs-DCP.

3.3. Morphology of blends and blend nanocomposites

Figure 4 shows the SEM micrographs of PLA/HDPE and PLA/HDPE-DCP blends. The PLA/HDPE blend exhibits typical type I cocontinuous morphology, as suggested by Marin and Favis [31]. For the PLA/HDPE-DCP blend, type II cocontinuous morphology, featured by laminar and thread-like components [31], is observed. The DCP is expected to compatibilize the PLA and HDPE components via initiating radical reactions between molecular chains of both components [33–34]. Thus, the appearance of type II cocontinuous morphology is ascribed to the improved compatibility between PLA and HDPE components. The SEM micrographs of PVCNTs, PVCNTs-DCP, and PCNTs-DCP are shown in Figure 5. As can be seen in Figures 5a–5c, all three PVCNTs show sea-island morphology, despite more elongated PLA droplets being observed at higher content of VCNTs. This is quite different from the morphology of PLA/HDPE blend, in which cocontinuous morphology is observed. It is clear that the presence of VCNTs causes the transformation of cocontinuous morphology to sea-island morphology, presumably via varying

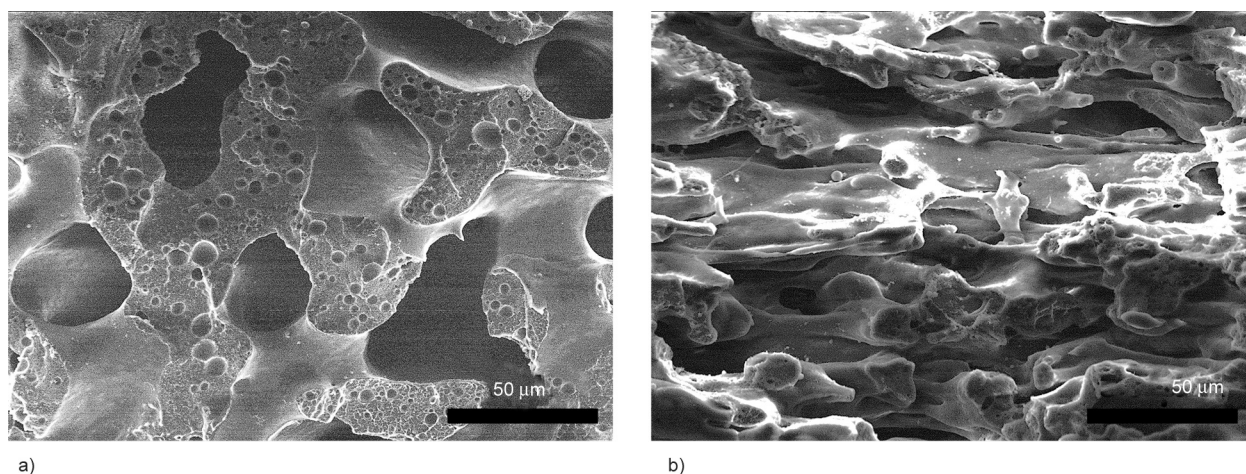


Figure 4. SEM micrographs of cryo-fractured surfaces of (a) PLA/HDPE and (b) PLA/HDPE-DCP blends.

viscosity ratios of PLA and HDPE components, and hindering the coalescence of PLA droplets [35, 36]. As can be clearly seen from Figures 5d–5i, cocontinuous morphology appears again in both PVCNTs-DCP and PCNTs-DCP. All the blend nanocomposites

seem to show type II cocontinuous morphology with laminar and thread-like HDPE components. It can be deduced that the presence of DCP facilitates the formation of type II cocontinuous morphology, whether CNTs or VCNTs are added. However, the

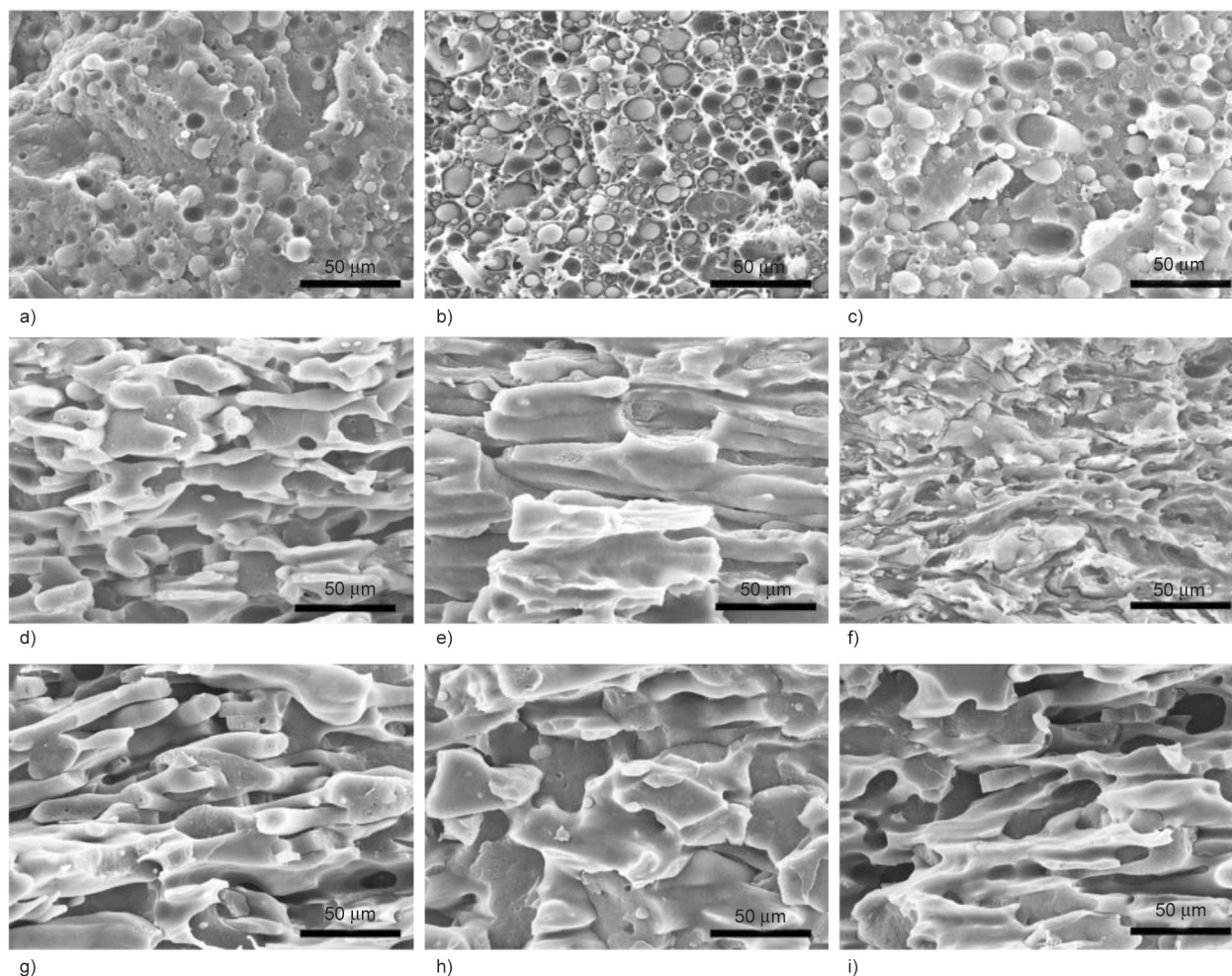


Figure 5. SEM micrographs of cryo-fractured surfaces of (a–c) PLA/HDPE/VCNTs, (d–f) PLA/HDPE/VCNTs-DCP, and (g–i) PLA/HDPE/CNTs-DCP blend nanocomposites. Content of VCNTs: (a, d, g) 0.5 wt%, (b, e, h) 1.0 wt%, and (c, f, i) 2.0 wt%.

compatibilizing efficiency of DCP on the PLA/HDPE blend is obviously higher in the presence of VCNTs. This can be evidenced by the obviously smaller phase sizes in PVCNTs-DCP (Figures 5d–5f), compared to PCNTs-DCP filled with the same content of CNTs (Figures 5g–5i).

3.4. Linear viscoelastic behaviors of blends and blend nanocomposites

To further investigate the compatibilizing efficiency and interfacial interactions, linear viscoelastic behaviors of PLA/HDPE blend, PLA/HDPE-DCP blend, and the three kinds of blend nanocomposites were measured. It has been well demonstrated that nanoparticles filled polymer blend exhibits higher storage modulus (G') than the unfilled polymer blend due to the contribution of interfacial storage modulus [37, 38]. As can be seen in Figure 6, both G' and loss modulus (G'') of PVCNTs, PVCNTs-DCP, and PCNTs-DCP is higher than that of PLA/HDPE and PLA/HDPE-DCP blends in the tested frequency range. However, the increments of G' and G'' are quite different for the three kinds of blend nanocomposites, especially at low frequencies. This can be mainly ascribed to the different intensities of interfacial interactions in the three kinds of blend nanocomposites.

For the PVCNTs, an obvious increase of G' at low frequencies is observed with incorporation of 0.5 wt% VCNTs, and further increase of G' can be observed with increasing the contents of VCNTs to 1.0 and 2.0 wt% (Figure 6a). Specifically, at 0.1 rad/s, the G' of P0.5VCNTs, P1.0VCNTs, and P2.0VCNTs is increased from 130.4 Pa (of PLA/HDPE blend) to 524.5, 902.6, and 1793.4 Pa, respectively. Since the VCNTs are mainly distributed in the HDPE phase, the hydrophobic interactions between HDPE chains and vinyl groups on the surfaces of VCNTs are responsible for the obviously increased G' at low frequencies [39, 40].

For the PVCNTs-DCP, a remarkable increase of G' is observed (Figure 6b). At 0.1 rad/s, the G' of P0.5VCNTs-DCP, P1.0VCNTs-DCP, and P2.0VCNTs-DCP is increased from 130.4 Pa (of PLA/HDPE blend) to 688.1, 2716.3, and 6132.4 Pa, respectively. In the presence of DCP, an increase of two orders of magnitude in G' is achieved by adding only 1.0 wt% of VCNTs; whereas an increase of only one order of magnitude in G' is achieved by adding 2.0 wt% of VCNTs if the DCP is absent. Pronounced

increase of G' has been reported for polymer blends reactively compatibilized using Janus particles due to strong interfacial interactions [41, 42]. In this work, the VCNTs are expected to act as reactive compatibilizers with the aid of DCP initiated radical reactions [22, 43]. That is, VCNTs may simultaneously react with both PLA and HDPE macromolecular radicals, leading to strong interfacial interactions among VCNTs, PLA phase, and HDPE phase.

One may doubt that the remarkably increased G' of PVCNTs-DCP is merely due to the DCP initiated crosslinking of PLA and HDPE chains. However, the possibility can be excluded since the G' of PLA/HDPE-DCP blend is only slightly higher than those of PLA/HDPE blend at low frequencies. The other possibility is that remarkably increased G' of PVCNTs-DCP is the combined effects of both nanofillers (whether VCNTs or CNTs) and DCP initiated crosslinking of molecular chains, rather than the strong interfacial interactions. This possibility can also be excluded since the G' of PCNTs-DCP is even lower than that of PVCNTs (not to say that of PVCNTs-DCP) at low frequencies, for certain content of CNTs (Figure 6c). Specifically, at 0.1 rad/s, the G' of P0.5CNTs-DCP, P1.0CNTs-DCP, and P2.0CNTs-DCP are 407.3, 437.7, and 753.2 Pa, respectively. Consequently, it is reasonable that strong interfacial interactions are achieved via the DCP initiated radical reactions among VCNTs, PLA chains, and HDPE chains. This makes VCNTs act as reactive compatibilizers for PLA and HDPE components, as is schematically shown in Figure 7.

3.5. Thermal behaviors of blends and blend nanocomposites

Figure 8 exhibits the DSC cooling and heating curves of PLA/HDPE blend, PLA/HDPE-DCP blend, and the three kinds of blend nanocomposites. It can be seen from Figures 8a–8c that the peak temperatures of crystallizing (T_c) of HDPE components are increased by 2–3 °C with the incorporation of VCNTs or CNTs, regardless of the presence of DCP. This can be ascribed to the nucleating effects of CNTs and VCNTs on the crystallization of PE [44–46]. For the PLA, usually, no crystallizing peaks can be observed due to low chain mobility [47, 48]. Herein, even if the PLA component can crystallize during DSC cooling, its crystallizing peak is still hard to be distinguished since it will overlap with that of HDPE components.

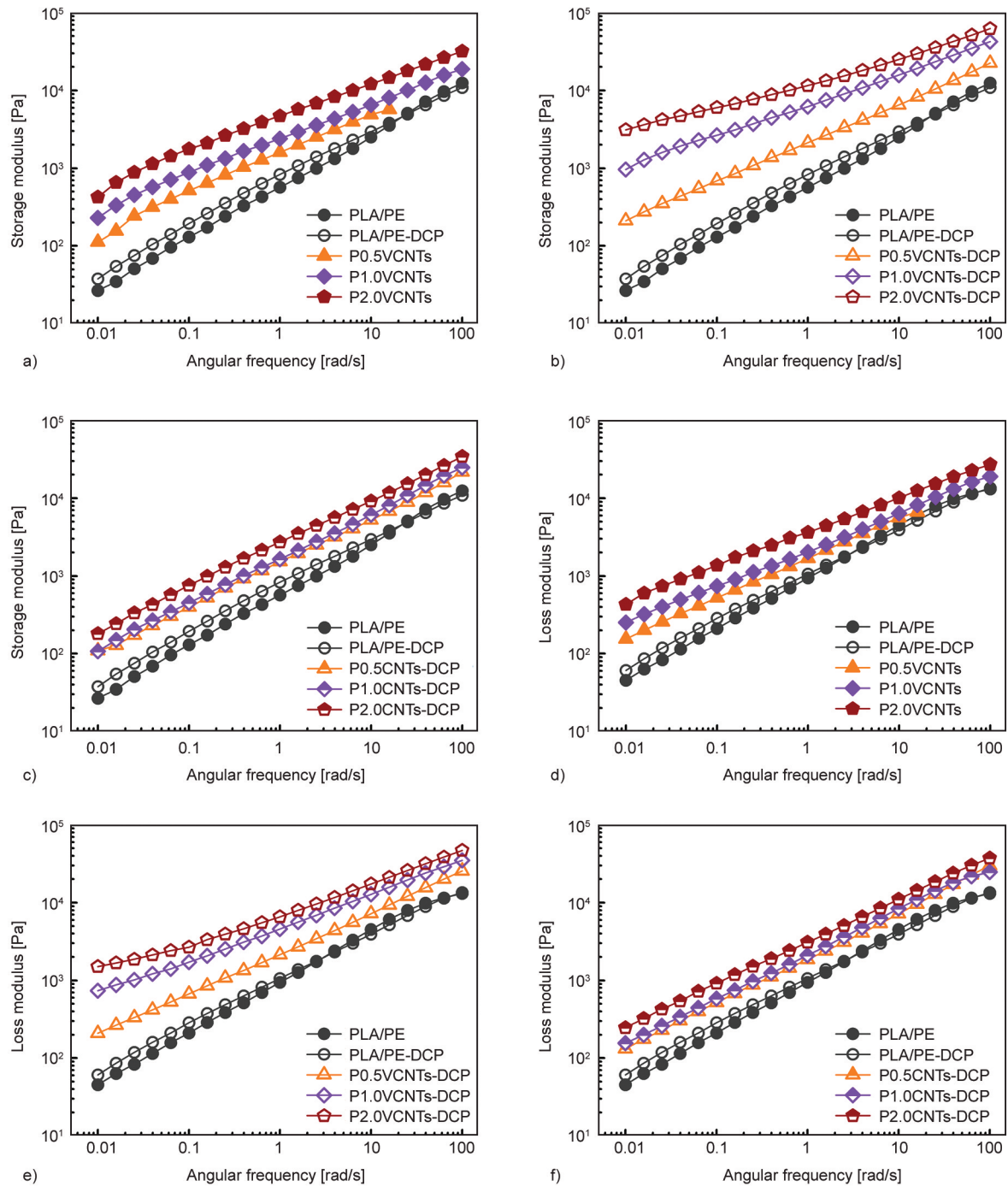


Figure 6. Storage modulus *versus* frequency curves of (a) PLA/HDPE/VCMNTs, (b) PLA/HDPE/VCMNTs-DCP, and (c) PLA/HDPE/CNTs-DCP blend nanocomposites; Loss modulus *versus* frequency curves of (d) PLA/HDPE/VCMNTs, (e) PLA/HDPE/VCMNTs-DCP, and (f) PLA/HDPE/CNTs-DCP blend nanocomposites.

Figures 8d–8f show the DSC heating curves of PLA/HDPE blend, PLA/HDPE-DCP blend, and the three kinds of blend nanocomposites. The cold crystallizing temperature ($T_{c,c}$), melting temperature (T_m), and crystallinity of PLA components are obtained from Figures 8d–8f and are listed in Table 1. It is interesting to find that P2.0VCNTs-DCP shows no cold crystallizing peak. Its crystallinity is calculated to be

33.8%, which is obviously higher than those of other blends and blend nanocomposites. This can be attributed to the fact that VCMNTs can act as nucleating agents of PLA in case of strong interfacial interactions. At a VCMNTs content of 2.0 wt%, the P2.0VCNTs-DCP can complete crystallization during melt cooling, and thus no cold crystallizing peak can be observed upon heating.

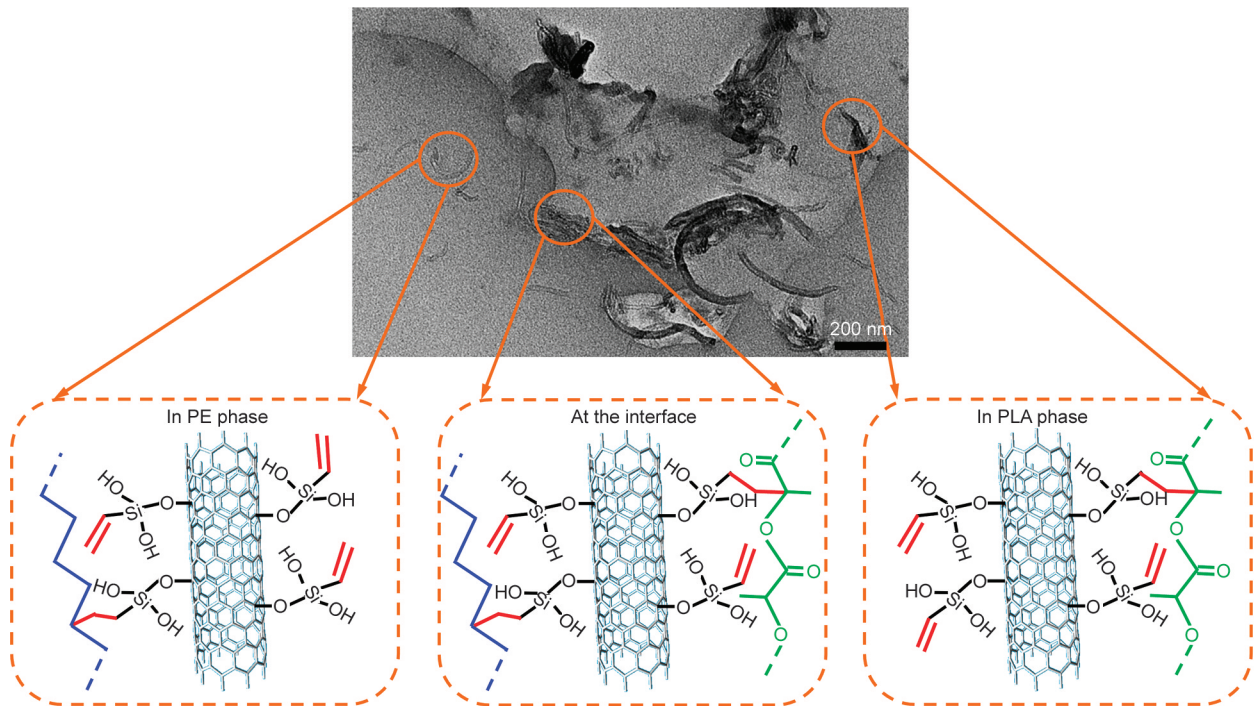


Figure 7. Schematics of enhancing interfacial interactions by radical reactions among VCNTs, PLA chains, and HDPE chains in PLA/HDPE/VCNTs blend nanocomposites.

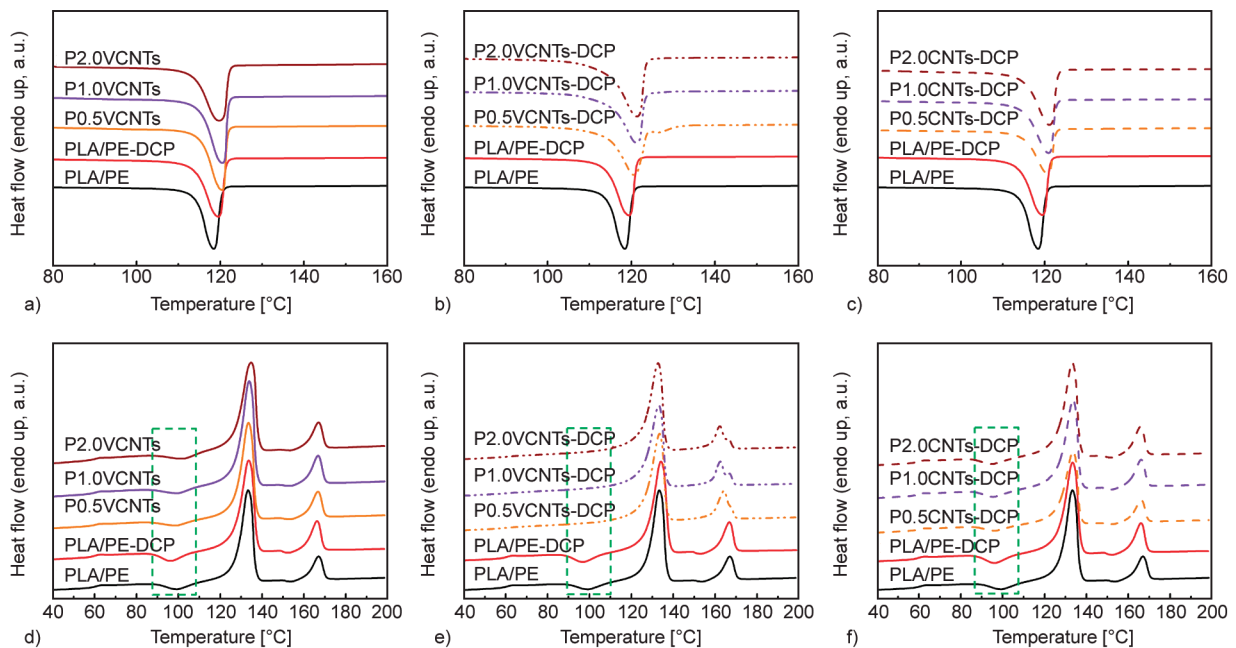


Figure 8. DSC cooling curves of (a) PLA/HDPE/VCNTs, (b) PLA/HDPE/VCNTs-DCP, and (c) PLA/HDPE/CNTs-DCP blend nanocomposites; DSC heating curves of (d) PLA/HDPE/VCNTs, (e) PLA/HDPE/VCNTs-DCP, and (f) PLA/HDPE/CNTs-DCP blend nanocomposites.

Figures 9a–9c show the DMA storage modulus (E') curves of PLA/HDPE blend, PLA/HDPE-DCP blend, and the three kinds of blend nanocomposites. A sharp decrease of E' is observed between 60 and 80 °C for all blends and blend nanocomposites due to the glass transition of PLA components [49]. After that, an

increase of E' is observed between 80 and 100 °C for all blends and blend nanocomposites except for P2.0VCNTs-DCP, as can be clearly seen from the images at the top right corner of Figures 9a–9c. The increase of E' in this temperature range is due to the cold crystallization of PLA component [50].

Table 1. Transition temperatures, enthalpies, and crystallinity of PLA component in PLA/HDPE/VCNTs, PLA/HDPE/VCNTs-DCP, and PLA/HDPE/CNTs-DCP blend nanocomposites.

Specimens	$T_{c,s}$, PLA [°C]	T_m , PLA [°C]	$\Delta H_{c,s}$, PLA [J/g]	ΔH_m , PLA [J/g]	Crystallinity of PLA [%]
PLA/HDPE	99.7	167.6	11.1	14.8	8.0
PLA/HDPE-DCP	96.9	166.8	11.7	17.3	12.0
P0.5VCNTs	99.7	167.2	10.7	14.2	7.6
P1.0VCNTs	99.7	167.1	10.4	13.8	7.4
P2.0VCNTs	99.9	167.1	11.0	14.3	7.2
P0.5VCNTs-DCP	95.5	166.6	9.8	16.1	13.6
P1.0VCNTs-DCP	94.8	165.6	7.8	16.5	18.9
P2.0VCNTs-DCP	–	165.4	–	15.4	33.8
P0.5CNTs-DCP	96.7	167.0	9.2	14.7	11.9
P1.0CNTs-DCP	95.9	166.8	8.6	14.9	13.2
P2.0CNTs-DCP	95.9	166.5	9.1	15.8	14.7

P2.0VCNTs-DCP exhibits a monotonous decrease of E' in the temperature range of 80 to 120 °C, corresponding to the fact that no cold crystallizing peak is observed on its DSC heating curve. Due to much higher crystallinity, P2.0VCNTs-DCP shows much higher E' than other blends and blend nanocomposites in the glass transition temperature range of PLA. Figures 9d–9f show the tan delta curves of PLA/HDPE blend, PLA/HDPE-DCP blend, and the three kinds of blend nanocomposites. The information about interfacial interactions in blends and blend nanocomposites can be obtained by analyzing the peak position, peak intensity, and peak width of tan delta curves [51, 52]. The peaks of PVCNTs are located almost at the same temperature (66.9 °C) as that of PLA/HDPE blend (Figure 9d). But the peak intensities of PVCNTs are slightly lower than that of PLA/HDPE blend due to hydrophobic interactions between VCNTs and HDPE chains. Note that the peak intensity of PLA/HDPE-DCP blend is obviously higher than that of PLA/HDPE blend. This can be ascribed to the larger energy dissipating at the interface of cocontinuous laminar and thread-like PLA and HDPE phases in the PLA/HDPE-DCP blend. For a similar reason, the peak intensities of P0.5VCNTs-DCP and PCNTs-DCP are obviously higher than that of PLA/PE blend (Figures 9e and 9f), which are comparable with that of PLA/HDPE-DCP blend. For the P2.0VCNTs-DCP, however, its peak intensity is obviously lowered than that of PLA/HDPE blend. Moreover, its peak is shifted from 66.9 to 71.2 °C, and its peak width is also obviously widened, indicating strong interfacial interactions and thick interfacial areas in P2.0VCNTs-DCP [53].

3.6. Tensile properties of blends and blend nanocomposites

Figure 10 shows the stress-strain curves, tensile strength, and elongation at break of PLA/HDPE blend, PLA/HDPE-DCP blend, and the three kinds of blend nanocomposites. PLA/HDPE blend exhibits a tensile strength of 12.6 MPa and an elongation at a break of 14.4%. The addition of DCP shows marginal improvements of the tensile strength but decreases the elongation at break. The PVCNTs exhibit tensile strength around 25.0 MPa, similar to that of pure HDPE [54]. This can be mainly due to their sea-island morphology, in which the HDPE acts as the matrix. However, their elongation at break is only in the range of 18 to 28% due to the weak interfacial interactions between HDPE matrix and dispersed PLA droplets.

For the PVCNTs-DCP, the increased trend of tensile strength is observed, as the content of VCNTs is increased from 0.5 to 2.0 wt%. The tensile strength of P0.5VCNTs-DCP, P1.0VCNTs-DCP, and P2.0VCNTs-DCP is 15.2, 23.7, and 25.9 MPa, respectively. This increase of tensile strength can be ascribed to the stronger interfacial interactions in PVCNTs-DCP with higher content of VCNTs. For the PCNTs-DCP, however, a decreasing trend of tensile strength is observed, as the content of CNTs is increased from 0.5 to 2.0 wt%. This can be due to a more severe aggregation of CNTs at a higher content. The elongation at break of PVCNTs-DCP and PCNTs-DCP is only in the range of 10 to 18%, which is slightly higher than that of pure PLA [55], but far lower than that of pure HDPE.

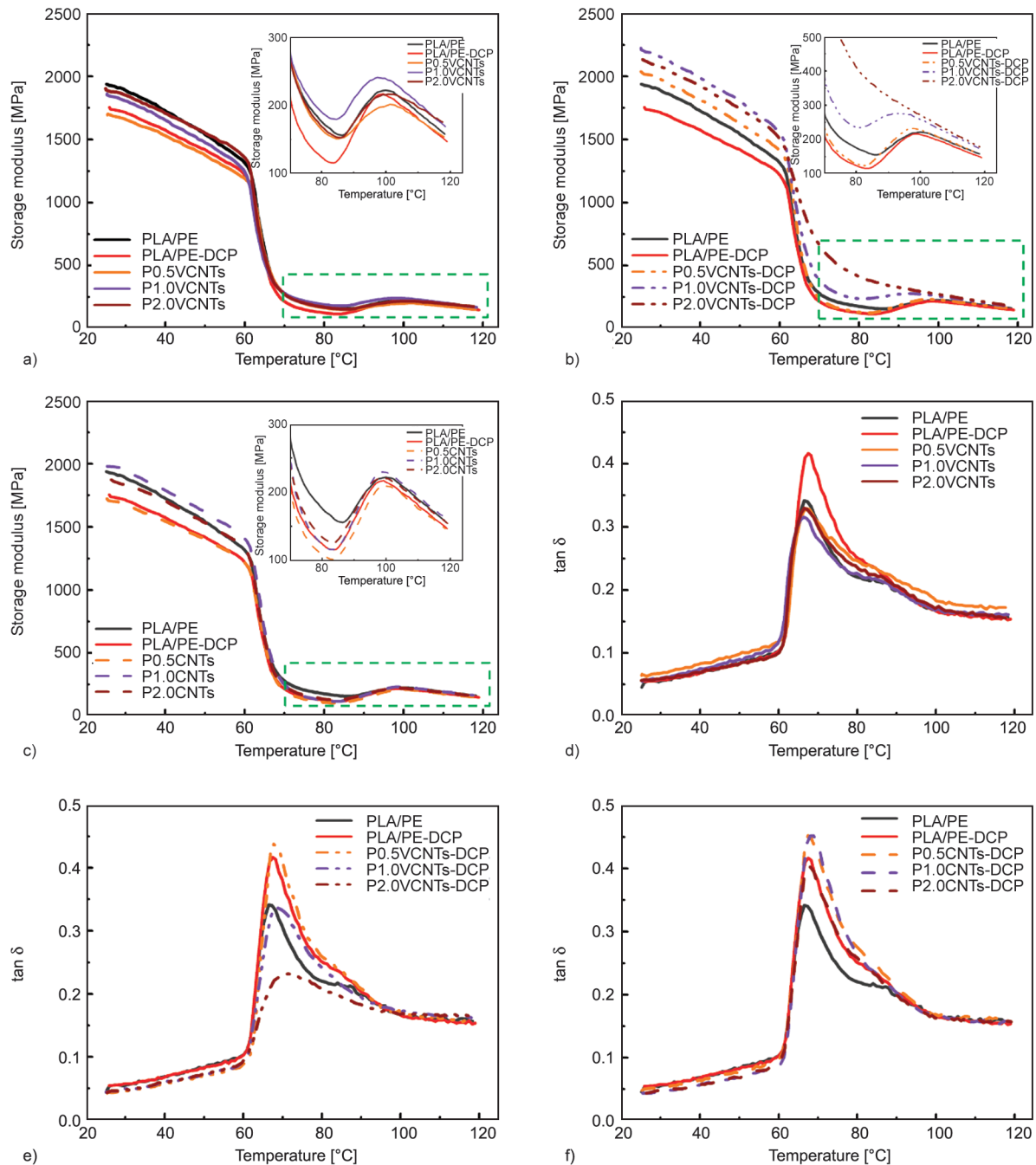


Figure 9. DMA storage modulus curves of (a) PLA/HDPE/VCNTs, (b) PLA/HDPE/VCNTs-DCP, and (c) PLA/HDPE/CNTs-DCP blend nanocomposites; DMA tan delta curves of (d) PLA/HDPE/VCNTs, (e) PLA/HDPE/VCNTs-DCP, and (f) PLA/HDPE/CNTs-DCP blend nanocomposites.

4. Conclusions

Vinylsilane grafted carbon nanotubes (VCNTs) are synthesized and are melt compounded with PLA/HDPE blends to prepare PLA/HDPE/VCNTs blend nanocomposites. In the presence of the DCP, the VCNTs can act as reactive compatibilizers for PLA/HDPE blends since both PLA and HDPE molecular radicals can react with the vinyl groups of VCNTs. For reactively compatibilized PLA/HDPE/VCNTs blend nanocomposites, the interfacial interactions

are obviously enhanced, as evidenced by the remarkably increased storage modulus at low frequencies. Moreover, the strong interfacial interactions can also be reflected by the DMA results, in which enhanced storage modulus and lowered peak intensity of $\tan \delta$ are observed for reactively compatibilized PLA/HDPE/VCNTs blend nanocomposites. Interestingly, at a VCNTs content of 2.0 wt%, the PLA component in reactively compatibilized PLA/HDPE/VCNTs blend nanocomposites can reach high crystallinity

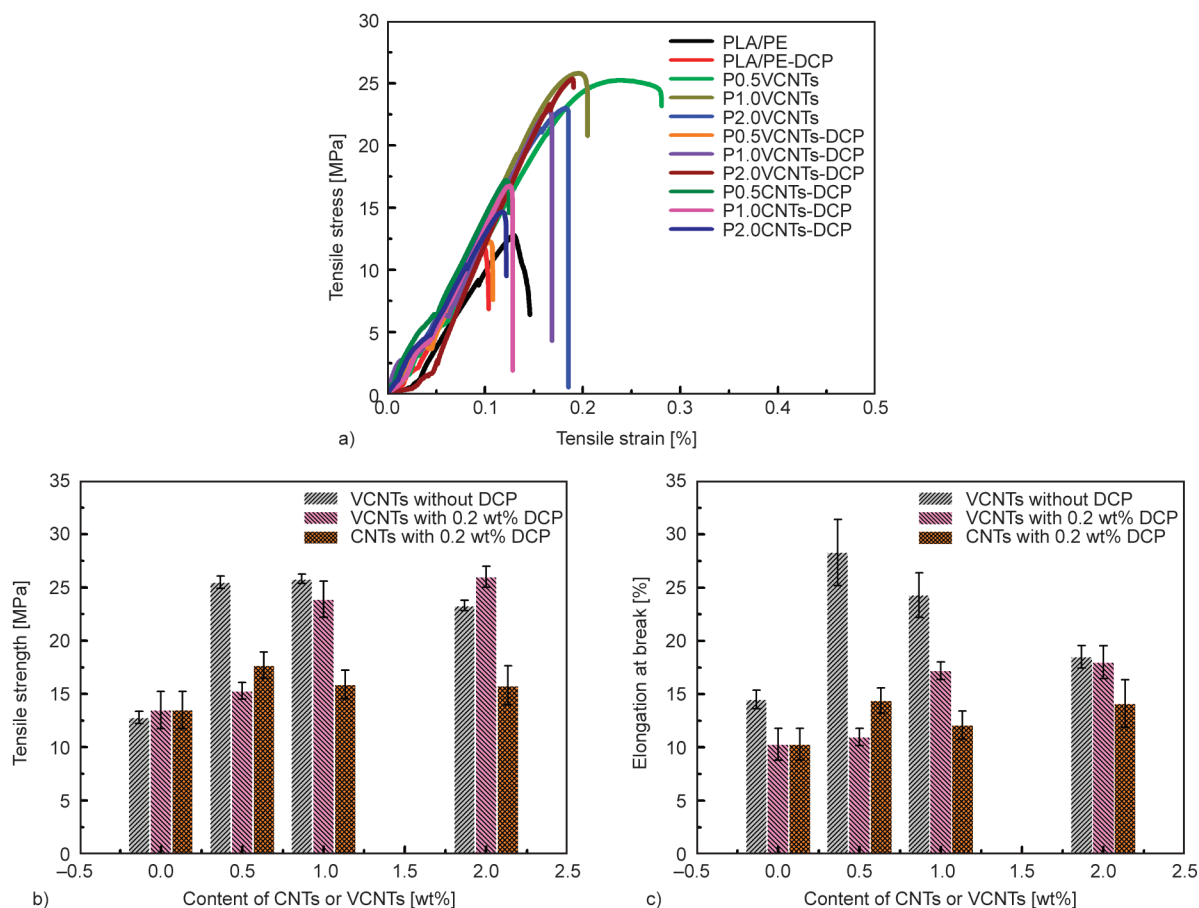


Figure 10. (a) Stress-strain curves, (b) tensile strength, and (c) elongation at break of PLA/HDPE/VCNTs, PLA/HDPE/VCNTs-DCP, and PLA/HDPE/CNTs-DCP blend nanocomposites.

(33.8%) after melt cooling. This is ascribed to the high nucleating efficiency of VCNTs on PLA, thanks to the strong interfacial interactions.

Acknowledgements

This work is financially supported by the National Natural Science Foundation of China (Grant Nos. 51605086, 12002315), Zhejiang Provincial Natural Science Foundation (No. LQ20A020003).

References

- [1] Deng S., Bai H., Liu Z., Zhang Q., Fu Q.: Toward supertough and heat-resistant stereocomplex-type polylactide/elastomer blends with impressive melt stability via *in situ* formation of graft copolymer during one-pot reactive melt blending. *Macromolecules*, **52**, 1718–1730 (2019).
<https://doi.org/10.1021/acs.macromol.8b02626>
- [2] de Kort G. W., Rastogi S., Wilsens C. H. R. M.: Controlling processing, morphology, and mechanical performance in blends of polylactide and thermotropic polyesters. *Macromolecules*, **52**, 6005–6017 (2019).
<https://doi.org/10.1021/acs.macromol.9b01083>
- [3] Wang H., Wei B., Gu X., Lin T., Li Y.: Determining the optimal molecular architecture for reactive splicing compatibilization: Toward a better understanding of reactive polymer processing. *Polymer*, **208**, 122948 (2020).
<https://doi.org/10.1016/j.polymer.2020.122948>
- [4] Zhang C-L., Li C., Wang L., Feng L-F., Lin T.: Dual effects of compatibilizer on the formation of oriented ribbon-like dispersed phase domains in polystyrene/polyamide 6 blends. *Chemical Engineering Science*, **17**, 146–156 (2018).
<https://doi.org/10.1016/j.ces.2017.12.008>
- [5] Wu W., Wu C., Peng H., Sun Q., Zhou L., Zhuang J., Cao X., Roy V. A. L., Li R. K. Y.: Effect of nitrogen-doped graphene on morphology and properties of immiscible poly(butylene succinate)/polylactide blends. *Composites Part B: Engineering*, **113**, 300–307 (2017).
<https://doi.org/10.1016/j.compositesb.2017.01.037>
- [6] Alkhodairi H., Russell S. T., Pribyl J., Benicewicz B. C., Kumar S. K.: Compatibilizing immiscible polymer blends with sparsely grafted nanoparticles. *Macromolecules*, **53**, 10330–10338 (2020).
<https://doi.org/10.1021/acs.macromol.0c02108>

- [7] Tian H., Tang Z., Zhuang X., Chen X., Jing X.: Biodegradable synthetic polymers: Preparation, functionalization and biomedical application. *Progress in Polymer Science*, **37**, 237–280 (2012).
<https://doi.org/10.1016/j.progpolymsci.2011.06.004>
- [8] Silva A. P. B., Montagna L. S., Passador F. R., Rezende M. C., Lemes A. P.: Biodegradable nanocomposites based on PLA/PHBV blend reinforced with carbon nanotubes with potential for electrical and electromagnetic applications. *Express Polymer Letters*, **15**, 987–1003 (2021).
<https://doi.org/10.3144/expresspolymlett.2021.79>
- [9] Lim L-T., Auras R., Rubino M.: Processing technologies for poly(lactic acid). *Progress in Polymer Science*, **33**, 820–852 (2008).
<https://doi.org/10.1016/j.progpolymsci.2008.05.004>
- [10] Anderson K. S., Lim S. H., Hillmyer M. A.: Toughening of polylactide by melt blending with linear low-density polyethylene. *Journal of Applied Polymer Science*, **89**, 3757–3768 (2003).
<https://doi.org/10.1002/app.12462>
- [11] Thurber C. M., Xu Y., Myers J. C., Lodge T. P., Macosko C. W.: Accelerating reactive compatibilization of PE/PLA blends by an interfacially localized catalyst. *ACS Macro Letters*, **4**, 30–33 (2015).
<https://doi.org/10.1021/mz500770y>
- [12] Milovanović V. L., Hajdinjak I., Lovriša I., Vrsaljko D.: The influence of the dispersed phase on the morphology, mechanical and thermal properties of PLA/PE-LD and PLA/PE-HD polymer blends and their nanocomposites with TiO₂ and CaCO₃. *Polymer Engineering and Science*, **59**, 1395–1408 (2019).
<https://doi.org/10.1002/pen.25124>
- [13] Castro D. O., Passador F., Ruvalo-Filho A., Frollini E.: Use of castor and canola oils in ‘biopolyethylene’ curauá fiber composites. *Composites Part A: Applied Science and Manufacturing*, **95**, 22–30 (2017).
<https://doi.org/10.1016/j.compositesa.2016.12.024>
- [14] Castro D. O., Ruvalo-Filho A., Frollini E.: Materials prepared from biopolyethylene and curaua fibers: Composites from biomass. *Polymer Testing*, **31**, 880–888 (2012).
<https://doi.org/10.1016/j.polymertesting.2012.05.011>
- [15] Anderson K. S., Hillmyer M. A.: The influence of block copolymer microstructure on the toughness of compatibilized polylactide/polyethylene blends. *Polymer*, **45**, 8809–8823 (2004).
<https://doi.org/10.1016/j.polymer.2004.10.047>
- [16] Wang Y., Hillmyer M. A.: Polyethylene-poly(L-lactide) diblock copolymers: Synthesis and compatibilization of poly(L-lactide)/polyethylene blends. *Journal of Polymer Science Part A: Polymer Chemistry*, **39**, 2755–2766 (2001).
<https://doi.org/10.1002/pola.1254>
- [17] Xu Y., Loi J., Delgado P., Topolkaraev V., McEneaney R. J., Macosko C. W., Hillmyer M. A.: Reactive compatibilization of polylactide/polypropylene blends. *Industrial and Engineering Chemical Research*, **54**, 6108–6114 (2015).
<https://doi.org/10.1021/acs.iecr.5b00882>
- [18] Zolali A. M., Favis B. D.: Toughening of cocontinuous polylactide/polyethylene blends *via* an interfacially percolated intermediate phase. *Macromolecules*, **51**, 3572–3581 (2018).
<https://doi.org/10.1021/acs.macromol.8b00464>
- [19] Wang H., Fu Z., Zhao X., Li Y., Li J.: Reactive nanoparticles compatibilized immiscible polymer blends: Synthesis of reactive SiO₂ with long poly(methyl methacrylate) chains and the *in situ* formation of Janus SiO₂ nanoparticles anchored exclusively at the interface. *ACS Applied Materials and Interfaces*, **9**, 14358–14370 (2017).
<https://doi.org/10.1021/acsami.7b01728>
- [20] Walther A., Matussek K., Müller A. H. E.: Engineering nanostructured polymer blends with controlled nanoparticle location using Janus particles. *ACS Nano*, **2**, 1302–1305 (2008).
<https://doi.org/10.1021/nn800108y>
- [21] Zhang J., Grzybowski B. A., Granick S.: Janus particle synthesis, assembly, and application. *Langmuir*, **33**, 6964–6977 (2017).
<https://doi.org/10.1021/acs.langmuir.7b01123>
- [22] Wang B., Peng D., Lv R., Na B., Liu H., Yu Z.: Generic melt compounding strategy using reactive graphene towards high performance polyethylene/graphene nanocomposites. *Composites Science and Technology*, **177**, 1–9 (2019).
<https://doi.org/10.1016/j.compscitech.2019.04.013>
- [23] Sung C. M., Kim M. J., Cobos M., Gu L., Macosko C. W.: Strategies for interfacial localization of graphene/polyethylene-based cocontinuous blends for electrical percolation. *AIChE Journal*, **65**, e16579 (2019).
<https://doi.org/10.1002/aic.16579>
- [24] Shen Q-J., Liu X-B., Jin W-J.: Solubility increase of multi-walled carbon nanotubes in water. *Carbon*, **28**, 526–563 (2013).
<https://doi.org/10.1016/j.carbon.2013.04.022>
- [25] Mihai M., Huneault M. A., Favis B. D., Li H.: Extrusion foaming of semi-crystalline PLA and PLA/thermo-plastic starch blends. *Macromolecular Bioscience*, **7**, 907–920 (2007).
<https://doi.org/10.1002/mabi.200700080>
- [26] Xie Y., Hill C. A. S., Xiao Z., Militz H., Mai C.: Silane coupling agents used for natural fiber/polymer composites: A review. *Composites Part A: Applied Science and Manufacturing*, **41**, 806–819 (2010).
<https://doi.org/10.1016/j.compositesa.2010.03.005>

- [27] Zhou T., Wang X., Liu X. H., Lai J. Z.: Effect of silane treatment of carboxylic-functionalized multi-walled carbon nanotubes on the thermal properties of epoxy nanocomposites. *Express Polymer Letters*, **4**, 217–226 (2010).
<https://doi.org/10.3144/expresspolymlett.2010.28>
- [28] Wang Y., Song C., Yu X., Liu L., Han Y., Chen J., Fu J.: Thermo-responsive hydrogels with tunable transition temperature crosslinked by multifunctional graphene oxide nanosheets. *Composites Science and Technology*, **151**, 139–146 (2017).
<https://doi.org/10.1016/j.compscitech.2017.08.016>
- [29] Jorio A., Saito R.: Raman spectroscopy for carbon nanotube applications. *Journal of Applied Physics*, **129**, 021102 (2021).
<https://doi.org/10.1063/5.0030809>
- [30] Wu D., Zhang Y., Zhang M., Yu W.: Selective localization of multiwalled carbon nanotubes in poly(ϵ -caprolactone)/polylactide blend. *Biomacromolecules*, **10**, 417–424 (2009).
<https://doi.org/10.1021/bm801183f>
- [31] Marin N., Favis B. D.: Co-continuous morphology development in partially miscible PMMA/PC blends. *Polymer*, **43**, 4723–4731 (2002).
[https://doi.org/10.1016/S0032-3861\(02\)00280-X](https://doi.org/10.1016/S0032-3861(02)00280-X)
- [32] Semba T., Kitagawa K., Ishiaku U. S., Kotaki M., Hamada H.: Effect of compounding procedure on mechanical properties and dispersed phase morphology of poly(lactic acid)/polycaprolactone blends containing peroxide. *Journal of Applied Polymer Science*, **103**, 1066–1074 (2007).
<https://doi.org/10.1002/app.25311>
- [33] Ma P., Cai X., Zhang Y., Wang S., Dong W., Chen M., Lemstra P. J.: *In-situ* compatibilization of poly(lactic acid) and poly(butylene adipate-co-terephthalate) blends by using dicumyl peroxide as a free-radical initiator. *Polymer Degradation and Stability*, **102**, 145–151 (2014).
<https://doi.org/10.1016/j.polymdegradstab.2014.01.025>
- [34] Zytner P., Wu F., Misra M., Mohanty A. K.: Toughening of biodegradable poly(3-hydroxybutyrate-co-3-hydroxyvalerate)/poly(ϵ -caprolactone) blends by *in situ* reactive compatibilization. *ACS Omega*, **5**, 14900–14910 (2020).
<https://doi.org/10.1021/acsomega.9b04379>
- [35] Yu W., Zhou W., Zhou C.: Linear viscoelasticity of polymer blends with co-continuous morphology. *Polymer*, **51**, 2091–2098 (2010).
<https://doi.org/10.1016/j.polymer.2010.03.005>
- [36] Xiang F., Shi Y., Li X., Huang T., Chen C., Peng Y., Wang Y.: Cocontinuous morphology of immiscible high density polyethylene/polyamide 6 blend induced by multiwalled carbon nanotubes network. *European Polymer Journal*, **48**, 350–361 (2012).
<https://doi.org/10.1016/j.eurpolymj.2011.11.013>
- [37] Huang S., Bai L., Trifkovic M., Cheng X., Macosko C. W.: Controlling the morphology of immiscible cocontinuous polymer blends *via* silica nanoparticles jammed at the interface. *Macromolecules*, **49**, 3911–3918 (2016).
<https://doi.org/10.1021/acs.macromol.6b00212>
- [38] Genoyer J., Yee M., Soulestin J., Demarquette N.: Compatibilization mechanism induced by organoclay in PMMA/PS blends. *Journal of Rheology*, **61**, 613–626 (2017).
<https://doi.org/10.1122/1.4982701>
- [39] Wang L., Ando M., Kubota M., Ishihara S., Hikima Y., Ohshima M., Sekiguchi T., Sato A., Yano H.: Effects of hydrophobic-modified cellulose nanofibers (CNFs) on cell morphology and mechanical properties of high void fraction polypropylene nanocomposite foams. *Composites Part A: Applied Science and Manufacturing*, **98**, 166–173 (2017).
<https://doi.org/10.1016/j.compositesa.2017.03.028>
- [40] Sato A., Kabusaki D., Okumura H., Nakatani T., Nakatsubo F., Yano H.: Surface modification of cellulose nanofibers with alkenyl succinic anhydride for high-density polyethylene reinforcement. *Composites Part A: Applied Science and Manufacturing*, **83**, 72–79 (2016).
<https://doi.org/10.1016/j.compositesa.2015.11.009>
- [41] Wang H., Yang X., Fu Z., Zhao X., Li Y., Li J.: Rheology of nanosilica-compatible immiscible polymer blends: Formation of a ‘heterogeneous network’ facilitated by interfacially anchored hybrid nanosilica. *Macromolecules*, **50**, 9494–9506 (2017).
<https://doi.org/10.1021/acs.macromol.7b02143>
- [42] Zhao X., Wang H., Fu Z., Li Y.: Enhanced interfacial adhesion by reactive carbon nanotubes: New route to high-performance immiscible polymer blend nanocomposites with simultaneously enhanced toughness, tensile strength, and electrical conductivity. *ACS Applied Materials and Interfaces*, **10**, 8411–8416 (2018).
<https://doi.org/10.1021/acsami.8b01704>
- [43] Kald  s T., Tr  ger A., Berglund L. A., Malmstr  m E., Re G. L.: Molecular engineering of the cellulose-poly (caprolactone) bio-nanocomposite interface by reactive amphiphilic copolymer nanoparticles. *ACS Nano*, **13**, 6409–6420 (2019).
<https://doi.org/10.1021/acsnano.8b08257>
- [44] Li L., Wang W., Laird E. D., Li C. Y., Defaux M., Ivanov D. A.: Polyethylene/carbon nanotube nano hybrid shish-kebab obtained by solvent evaporation and thin-film crystallization. *Polymer*, **52**, 3633–3638 (2011).
<https://doi.org/10.1016/j.polymer.2011.05.006>
- [45] Minus M. L., Chae H. G., Kumar S.: Polyethylene crystallization nucleated by carbon nanotubes under shear. *ACS Applied Materials and Interfaces*, **4**, 326–330 (2012).
<https://doi.org/10.1021/am2013757>

- [46] Vega J. F., Martinez-Salazar J., Trujillo M., Arnal M. L., Müller A. J., Bredeau S., Dubois P.: Rheology, processing, tensile properties, and crystallization of polyethylene/carbon nanotube nanocomposites. *Macromolecules*, **42**, 4719–4727 (2009).
<https://doi.org/10.1021/ma900645f>
- [47] Xiao H., Lu W., Yeh J-T.: Effect of plasticizer on the crystallization behavior of poly(lactic acid). *Journal of Applied Polymer Science*, **113**, 112–121 (2009).
<https://doi.org/10.1002/app.29955>
- [48] Kulinski Z., Piorkowska E., Gadzinowska K., Stasiak M.: Plasticization of poly(L-lactide) with poly(propylene glycol). *Biomacromolecules*, **7**, 2128–2135 (2006).
<https://doi.org/10.1021/bm060089m>
- [49] Liu H., Chen N., Shan P., Song P., Liu X., Chen J.: Toward fully bio-based and supertough PLA blends *via in situ* formation of cross-linked biopolyamide continuity network. *Macromolecules*, **52**, 8415–8429 (2019).
<https://doi.org/10.1021/acs.macromol.9b01398>
- [50] Yu L., Liu H., Dean K., Chen L.: Cold crystallization and postmelting crystallization of PLA plasticized by compressed carbon dioxide. *Journal of Polymer Science Part B: Polymer Physics*, **46**, 2630–2636 (2008).
<https://doi.org/10.1002/polb.21599>
- [51] Maio A., Fucarino R., Khatibi R., Rosselli S., Bruno M., Scaffaro R.: A novel approach to prevent graphene oxide re-aggregation during the melt compounding with polymers. *Composites Science and Technology*, **119**, 131–137 (2015).
<https://doi.org/10.1016/j.compscitech.2015.10.006>
- [52] Yang Z., Xu Z., Zhang L., Guo B.: Dispersion of graphene in chlorosulfonated polyethylene by slurry compounding. *Composites Science and Technology*, **162**, 156–162 (2018).
<https://doi.org/10.1016/j.compscitech.2018.04.030>
- [53] Peng M., Xiao G., Tang X., Zhou Y.: Hydrogen-bonding assembly of rigid-rod poly(p-sulfophenylene terephthalamide) and flexible-chain poly(vinyl alcohol) for transparent, strong, and tough molecular composites. *Macromolecules*, **47**, 8411–8419 (2014).
<https://doi.org/10.1021/ma501590x>
- [54] Zhang H-X., Park J-H., Moon Y-K., Eun-Bin K., Zhang X-Q., Yoon K-B.: Preparation of polyethylene/graphene nanocomposites with octadecylamine-modified graphene oxide-MgCl₂-supported Ziegler–Natta catalyst. *Journal of Polymer Science Part A: Polymer Chemistry*, **55**, 855–860 (2017).
<https://doi.org/10.1002/pola.28437>
- [55] Piorkowska E., Kulinski Z., Galeski A., Masirek R.: Plasticization of semicrystalline poly(L-lactide) with poly(propylene glycol). *Polymer*, **47**, 7178–7188 (2006).
<https://doi.org/10.1016/j.polymer.2006.03.115>